Progress in Neuropsychopharmacology & Biological Psychiatry 84 (2018) 79–92

Contents lists available at ScienceDirect

Progress in Neuropsychopharmacology & Biological Psychiatry

journal homepage: www.elsevier.com/locate/pnp

Effect of distress on transient network dynamics and topological equilibrium in phantom sound perception

Anusha Mohan[a], Sandra Jovanovic Alexandra[a], Cliff V. Johnson[a], Dirk De Ridder[b], Sven Vanneste[a,*]

[a] Lab for Clinical & Integrative Neuroscience, School of Behavioral and Brain Sciences, The University of Texas at Dallas, USA
[b] Department of Surgical Sciences, Section of Neurosurgery, Dunedin School of Medicine, University of Otago, Dunedin, New Zealand

ARTICLE INFO

Keywords:
Metastability
Small-world
sLORETA
EEG
Functional connectivity

ABSTRACT

Distress is a domain-general behavioral symptom whose neural correlates have been under investigation for a long time now. Although some studies suggest that distress is encoded by changes in alpha activity and functional connectivity between specific brain regions, no study that we know has delved into the whole brain temporal dynamics of the distress component. In the current study, we compare the changes in the mean and variance of functional connectivity and small-worldness parameter over 3 min of resting state EEG to analyze the fluctuation in transient stable states, and network structure. On comparing these measures between healthy controls and patients experiencing low and high levels of distress due to a continuous ringing in the ear (tinnitus), we observe an increase in fluctuation between transient stable states characterized by an increase in both variance of functional connectivity and the small-worldness parameter. This results in a possible increase in degrees of freedom leading to a paradoxical equilibrium of the network structure in highly distressed patients. This may also be interpreted as a maladaptive compensation to look for information in order to reduce the hypersalience in highly distressed individuals. In addition, this is correlated with the amount of distress only in the high distress tinnitus group, suggesting a catastrophic breakdown of the brain's resilience. Distress not only accompanies tinnitus, but other disorders such as somatic disorders, fibromyalgia, post-traumatic stress disorder, etc. Since the current study focuses on a disorder-general distress symptom, the methods and results of the current study have a wide application in different neuropathologies.

1. Introduction

The brain is a complex system wherein brain areas are connected to one another in a specific cost-effective "small-world" topology that balances metabolic cost with efficiency of information transfer (Bullmore and Sporns, 2012; Sporns and Zwi, 2004). Such an organization coordinates two opposing functions: functional segregation versus functional integration (Watts and Strogatz, 1998). Functional segregation is the ability of the brain to carry out specialized processes in densely interconnected groups of brain regions or modules (Rubinov and Sporns, 2010). Conversely, functional integration is the ability of certain brain regions to rapidly combine information across different modules (Rubinov and Sporns, 2010). Empirically this is estimated using a measure called "small-worldness", calculated as the ratio between functional integration and segregation in comparison to a fully random network (Humphries and Gurney, 2008).

Previous studies have examined this balance in network topology only from the point of static functional connectivity, assuming the associations between brain regions are constant throughout the length of the functional recording using several neuroimaging techniques (Bassett and Bullmore, 2006; Humphries and Gurney, 2008; Sanz-Arigita et al., 2010). However, the brain is a dynamic entity whose functional connectivity and network organization constantly changes even across the length of the recording (Córdova-Palomera et al., 2017; Park et al., 2017). This property of the brain aids in rapid, efficient, and flexible communication across brain regions by opening multiple functional paths for information transfer (Deco and Kringelbach, 2016). Thus, functional integration and segregation, and the balance between the two, are also temporally varying parameters.

The balance between these temporally varying and functionally opposing network properties is proposed to be a direct consequence of the brain's ability to spontaneously and rapidly switch between multiple transient stable states, a characteristic known as metastability (Fingelkurts and Fingelkurts, 2004; Kelso and Tognoli, 2006; Shanahan,

* Corresponding author at: Lab for Clinical & Integrative Neuroscience, School of Behavioral & Brain Science, University of Texas at Dallas, 800 W Campbell Rd, Richardson, TX 75080, USA
E-mail address: sven.vanneste@utdallas.edu (S. Vanneste).

https://doi.org/10.1016/j.pnpbp.2018.01.025
Received 21 October 2017; Received in revised form 12 December 2017; Accepted 31 January 2018
Available online 02 February 2018
0278-5846/

2010; Tognoli and Kelso, 2014). Metastability is empirically measured as the variance of phase coherence of neural activity between brain regions over the length of the recording (Deco and Kringelbach, 2016; Váša et al., 2015). It is also directly related to the number of degrees of freedom in the brain, which is important in maintaining the critical balance between functional integration and segregation (Fingelkurts and Fingelkurts, 2004). In ecology, metastability was found to be directly related to the resilience of the system (Scheffer et al., 2015). Resilience is defined as the ability of a system to absorb disturbances and resist transformation from one regime to the other (Holling, 1973, 1996; Walker et al., 2004). From a behavioral perspective, resilience is defined as the ability to avoid deleterious behavioral changes in the presence of chronic stress (Russo et al., 2012). From these definitions of resilience, we may conclude that resilience is the property of a system to absorb disturbances and preserve its characteristics in the presence of a chronic stressor.

In the current study, we are interested in evaluating the disruption of the brain's metastability and in turn the balance between functional integration and segregation in the presence of a pathology, like tinnitus. Tinnitus is the continuous perception of a phantom sound in the absence of an external sound source (Jastreboff, 1990). Tinnitus was shown to be accompanied by changes in functional connectivity between cortical and subcortical regions in resting state networks (Husain and Schmidt, 2014). Increased functional connectivity was estimated between the auditory cortices and the amygdala in the tinnitus group when compared to age-matched normal hearing controls (Kim et al., 2012). Some other studies reported increased connectivity between the brainstem, cerebellum, basal ganglia, nucleus accumbens, parahippocampal areas, right frontal and parietal areas, left sensorimotor areas and left superior temporal region and a decrease in connectivity between the right primary auditory cortex, left fusiform gyrus, left frontal and bilateral occipital regions (Maudoux et al., 2012). Changes in activity and functional connectivity in and between auditory, non-auditory and limbic regions were also shown to be correlated with specific symptoms of tinnitus such as pitch of the percept (De Ridder et al., 2014, 2011b), loudness of the percept (De Ridder et al., 2015a), type e.g. pure tone or narrow-band noise (Vanneste et al., 2010b), laterality (Vanneste et al., 2011) and chronicity (Song et al., 2013). Hence, tinnitus was hypothesized to be segregated into different behavioral symptoms coded into multiple separable subnetworks that were integrated into a unified percept (De Ridder et al., 2014). In our previous studies we showed that tinnitus was accompanied by changes in functional connectivity not only between specific regions of interest but showed changes in whole brain network connectivity where the tinnitus network shifted to a lattice topology in the lower frequencies and a random topology in the higher frequencies (Mohan et al., 2016b). Further, the pathology could act as a stressor producing a chronic negative emotional component associated with several pathologies by different terms – annoyance, suffering or distress.

Distress is a domain-general symptom that accompanies several disorders such chronic pain, chronic tinnitus, post-traumatic stress disorder, dyspnea in asthma, social rejection, and in functional somatic syndromes such as electro-sensitivity to mobile phones etc. (Kross et al., 2007; Landgrebe et al., 2008; Moisset and Bouhassira, 2007; Vanneste et al., 2010a; von Leupoldt et al., 2009; Wager et al., 2013). Several studies have investigated the neural correlates of distress. Specifically, in tinnitus, distress is associated with increased activity in the dorsal, subgenual and pregenual anterior cingulate cortex, insula, parahippocampus, dorsal lateral prefrontal cortex, and the amygdala, mainly in the alpha (but also beta) frequency band (De Ridder et al., 2011a; Imperatori et al., 2014; Vanneste et al., 2010a; Weisz et al., 2005). Distress has also shown to be encoded by changes in static functional connectivity between these regions also mainly observed in the alpha (and beta) frequency bands (Chen et al., 2017; De Ridder et al., 2011a; Imperatori et al., 2014; Song et al., 2015; Vanneste et al., 2014). The alpha frequency band is physiologically associated with two processes, inhibition and timing that governs two basic qualities of top-down attention – suppression of irrelevant stimuli and selection of salient stimuli (Klimesch, 2012; Klimesch et al., 2007). Reduction in alpha power has been attributed to disinhibition in tinnitus and serves as an important neural marker of dysrhythmic thalamocortical oscillations (De Ridder et al., 2015b; Llinás et al., 1999). Further, the distress percept is hypothesized to be the behavioral manifestation of hypersalience, or increased top-down goal related attention that is also encoded in the alpha frequency band (De Ridder et al., 2014).

Although the neural correlates of distress are seemingly well investigated, there is still no study that examined the link between distress and the dynamic aspects of network equilibrium i.e. balance between functional integration and segregation, and the resilience of the brain. As mentioned before, distress is an integral part of various disorders and there have been several attempts to objectively quantify chronic distress to try and alleviate the emotional component of a disorder, but with little success. Thus, the current study investigates the association between distress and changes in the metastability of the brain, and dynamic changes in functional network topology using resting state EEG. Through this study we aim to establish the dynamic neural correlates of the distress/emotional percept of a disorder which can give us important insight into the dynamic changes in the brain in the presence of chronic distress and a tangible and objective parameter that may be clinically modified by means of invasive or non-invasive neuromodulation techniques. The dynamic aspect of metastability provides a more realistic and accurate correlate of brain functioning accounting for spatio-temporal changes in network topology. Further, the disorder-general nature of distress may allow the results of the current study to extrapolate to other disorders apart from tinnitus, defining a general correlate for chronic distress. Metastability is measured as the variance in functional connectivity between brain areas and is associated with the variance of the small-world parameter, which is used to characterize dynamic changes in functional network topology. The changes in mean and variance of the connectivity strength and the small-world parameter are compared between healthy controls and tinnitus subjects with low and high levels of distress, specifically in the alpha frequency bands. We hypothesize that distress will have a non-linear effect on the changes in mean and variance in functional connectivity and fluctuation of functional network topology, i.e. the changes will depend on the amount of distress experienced by the patients. We hypothesize that an increase or decrease in the variance of network connectivity will reflect corresponding changes in metastability, characterizing an increase or decrease in fluctuation between transient states. This in turn would characterize a change in fluctuation of the network topology which may be confirmed by an increase or decrease in the variance of the small-world parameter. Finally, we hypothesize that the relationship between metastability and distress will depend on the amount of distress perceived characterizing the resilience of the brain to the presence of the tinnitus stressor.

2. Materials and methods

2.1. Patients with an auditory phantom percept

The patient sample consisted of 151 patients (M = 45.87 years; SD = 13.25; 102 males and 43 females) all experiencing continuous tinnitus. The patient's condition was considered chronic if the onset of the tinnitus dated back a year or more. Patients with pulsatile tinnitus, Ménière disease, otosclerosis, chronic headache, neurological disorders such as brain tumors, and individuals being treated for mental disorders were excluded from the study. Audiometric tests consisted of pure tone audiometry, where hearing thresholds at 0.125 kHz, 0.25 kHz, 0.5 kHz, 1 kHz, 2 kHz, 3 kHz, 4 kHz, 6 kHz and 8 kHz were obtained according to the procedures prescribed by the British Society of Audiology (M = 23.28 dB HL, SD = 16.65) (Audiology, 2008). Further, the pitch and loudness of the tinnitus were recorded by performing a simple

analysis of the ear contralateral to the tinnitus ear in patients with unilateral tinnitus, and of the ear contralateral to the worst tinnitus ear in patients with bilateral tinnitus. A 1 kHz pure tone was presented to the ear contra lateral to the (worst) tinnitus ear at an intensity that was 10 dB above the patient's hearing threshold of that ear. The pitch of the perceived tinnitus was measured by adjusting the frequency of the tone to match the pitch of the perceived tinnitus. The perceived loudness was matched to the intensity of the tone in a similar way. The tinnitus loudness in dB SL was computed as the difference between the absolute tinnitus loudness in dB HL and the audiometric threshold at the tinnitus frequency (Meeus et al., 2011; Meeus et al., 2010). The perceived location of patients' tinnitus (left ear ($N = 43$), right ear ($N = 37$), both ears ($N = 47$), and centralized in the middle of the head (bilateral) as well the type of tinnitus (pure tone-like tinnitus ($N = 60$) or noise-like tinnitus ($N = 84$)) was noted. In addition to the audiological tests, patients also answered a set of questionnaires describing some of the subjective behavioral symptoms of tinnitus. A visual analogue scale (VAS) for loudness ('How loud is your tinnitus?': 0 = no tinnitus and 10 = as loud as imaginable') was assessed ($M = 5.50$, $SD = 2.45$). The Tinnitus Questionnaire (TQ) (Meeus et al., 2007) that measures a broad spectrum of tinnitus-related psychological complaints was administered. The global TQ score can be computed to measure the general level of psychological and psychosomatic distress ($M = 38.55$, $SD = 17.24$). Tinnitus patients were first subdivided into the low and high distress groups based on their Tinnitus Questionnaire scores. Patients with TQ score ≤ 46 were classified into the low distress group and patients with TQ score > 46 were classified into the high distress group. These thresholds are based on the clinical classification of different grades of distress in tinnitus - Slight (0–30 points; grade 1), moderate (31–46; grade 2), severe (47–59; grade 3), and very severe (60–84; grade 4) distress (Goebel and Hiller, 1994). Thus, patients suffering from grade 1 and grade 2 distress were classified into the low distress ($N = 91$) group, and patients suffering from grade 3 and grade 4 tinnitus were classified into the high distress group ($N = 45$). This study was approved by the local ethical committee (Antwerp University Hospital) and was in accordance with the declaration of Helsinki. Collection of the data was under approval of IRB UZA OGA85. All patients gave an informed consent.

2.2. Healthy control group

A healthy control group ($N = 125$; $M = 44.04$ years; $SD = 15.33$; 45 males and 80 females) was included in the study. None of these subjects were known to suffer from tinnitus of any kind. Subjects suffering from psychiatric or neurological illnesses, having a history of psychiatric or drug/alcohol abuse, history of head injury (with loss of consciousness) or seizures, headaches, or physical disabilities were excluded from the study. No hearing assessments were performed on the healthy controls. A summary of the demographics of the control and tinnitus group are given in Table 1.

Table 1
Demographics of participants in control and tinnitus group.

Demographics	Controls	Tinnitus
Number of participants	125	151
Age	44.04 ± 15.33 years	45.87 ± 13.25 years
Sex	45 M 80 F	102 M 43 F
Hearing loss	Not recorded	23.28 ± 16.65 dB HL
Tinnitus laterality		LE = 43; RE = 37; both = 47
Tinnitus type		PT = 60; NNB = 84
Tinnitus loudness (VAS)		5.50 ± 2.45
Tinnitus distress (TQ score)		38.55 ± 17.24

M = Male; F = Female; LE = Left ear; RE = Right ear; PT = Pure tone; NNB = Narrow band noise.

2.3. Data collection

Continuous resting state Electroencephalogram (EEG) data was obtained from both the tinnitus and control groups (sampling rate = 500 Hz, band passed 0.15–200 Hz). Subjects in both the groups were instructed to close their eyes for 5 min. The participants were seated upright on a comfortable chair in a fully-lit room. EEG data was collected using 19 electrodes (Fp1, Fp2, F7, F3, Fz, F4, F8, T7, C3, Cz, C4, T8, P7, P3, Pz, P4, P8, O1, O2) placed per the standard 10–20 International placement, sampled using Mitsar-201 amplifiers (NovaTech http://www.novatecheeg.com/) and referenced to digitally linked ears. Impedances on each of the electrodes were maintained below 5 kΩ. The data was re-sampled to 128 Hz and band-pass filtered in the range 2–44 Hz as a part of the off-line analysis. The data was then transposed into Eureka! software (Congedo, 2002), where it was carefully plotted and manually inspected for artifacts. Artifacts including eye-blinks, eye movements, teeth clenching, body movement, and ECG artifacts were removed from the EEG.

2.4. Time windows

After manual cleaning of EEG data, each participant had at least 3 min of continuous EEG data. The first 3 min of data was used for the participants who had > 3 min of data. The first 15 s of the data was disregarded and the next 2 min 45 s of stable EEG recording was considered for further analysis. The continuous stream of EEG was divided into 3 second epochs of overlapping and non-overlapping time windows. The overlapping time windows were constructed using a 1 second sliding window and the non-overlapping time windows were epoched back-to-back. This resulted in 163 epochs with overlapping sliding windows, and 55 epochs with non-overlapping sliding window. The functional connectivity was calculated in the overlapping 163 epochs and non-overlapping 55 epochs in the low and high alpha frequency bands as detailed below. A visual representation of dynamic functional connectivity between the 84 Brodmann areas in the three groups and two frequency bands within overlapping and non-overlapping sliding conditions are shown in the video included in supplementary material.

2.5. Source localization

Intracerebral electrical sources were estimated using the standardized low-resolution brain electromagnetic tomography (sLORETA; Pascual-Marqui, 2002) software. sLORETA is useful in computing the neuronal activity in current density (A/m^2) without assuming a predefined number of active sources. A common average reference transformation is performed even before the application of the source-localization algorithm (Pascual-Marqui, 2002). The solution space for the algorithm used in this study along with the lead field matrix are implemented in the LORETA-Key software (freely available at http://www.uzh.ch/keyinst/loreta.htm). This software applies the boundary element method on the MNI-152 (Montreal neurological institute, Canada) template of Mazziotta et al. (2001) to implement the revisited realistic electrode coordinates (Jurcak et al., 2007) and the lead field produced by Fuchs et al. (2002). Thus, the neocortical volume (including hippocampus and anterior cingulate cortex) in 6239 voxels, each having a 5 mm^3 thickness in MNI space, is divided and labeled by the sLORETA-key anatomical template based on probabilities returned by the Daemon Atlas (Lancaster et al., 2000). The 6239 voxels were distributed into 84 Brodmann areas which form the regions of interest for the current study. The position of the Brodmann areas used in the current study is shown in Fig. 1 and the abbreviations are expanded in Table 2. The following analyses were performed in 2 frequency bands defined as alpha1 (8–10 Hz), alpha2 (10–12 Hz).

Fig. 1. The 84 Brodmann areas used in the current study.

2.6. Lagged phase coherence and temporal variance

"Lagged phase coherence" between sources is interpreted as the amount of cross-talk between the regions contributing to the activity within the sources (Congedo et al., 2010). The cross-talk between the sources is equivalent to the information shared by axonal transmission owing to the coherent, lagged-phase oscillatory property of the sources. More precisely, the signal is decomposed into a finite series of sine and cosine waves which characterize the in-phase and out-of-phase carrier waves. The sine and cosine counterparts, form the real and imaginary part of the Fourier decomposition (Bloomfield, 2004). The lag of the cosine waves behind their respective sine counterparts is inversely proportional to their frequency, and accounts to a quarter of the period; for example, the period of a sinusoidal wave at 10 Hz is 100 ms. The cosine is shifted a quarter of a cycle (25 ms) with the respect to the sine. This would mean that the lagged phase coherence at 10 Hz indicates coherent oscillations with a 25 ms delay. The same at 20 Hz would indicate a delay of 12.5 ms, etc. The lagged phase coherence between each pair-wise combination of Brodmann area signifies the functional connectivity strength between them. The lagged phase coherence between pairs of 84 Brodmann areas were computed in each of the 163 epochs in the sliding window condition, and 55 epochs in the non-sliding window condition from the 2 groups in the 2 frequency bands defined above. The average connectivity strength of the network (average of all the connections in each epoch) and the average connectivity strength of each connection (average of the connectivity strength of pairwise Brodmann areas across epochs) were additionally calculated. The variance of the functional connectivity of the network and pairwise connection across the 163 epochs in the sliding window condition, and 55 epochs in the non-sliding window condition, served as a measure of metastability.

2.7. Small-world parameter

The small-world parameter is a graphic theoretical measure that empirically describes the topology of a given network. It is calculated as the ratio of the relative characteristic path length to the relative cluster coefficient. The closer the value of the small-worldness parameter is to 1, the more small-world the network; the greater the value of the small-worldness parameter, the more random the topology and the lesser the value of the small-worldness parameter the more ordered the topology (Humphries and Gurney, 2008).

The characteristic path length is defined as the length of the shortest path connecting any two nodes in the network. The connectivity strength matrix is converted to a connection length matrix by taking the inverse of the values of the functional connectivity strength. The functional distance between every pair of Brodmann areas is calculated using Dijkstra's algorithm (Dijkstra, 1959). Finally, the average of all the distances is calculated as the shortest path length of the network. The relative path length is the ratio of characteristic path length of the network to the characteristic path length of a random network. In the current study, the characteristic path length of the random network was calculated by averaging the characteristic path length of 300 random networks.

The cluster coefficient is a measure that describes the strength of connectivity among neighboring nodes. It is calculated by estimating the number of triangles around a node. The relative cluster coefficient is the ratio of the cluster coefficient of the network to the cluster coefficient of a random network. In the current study, the cluster coefficient of the random network was calculated by averaging the cluster coefficient length of 300 random networks.

The characteristic path length and cluster coefficient of the control, low distress, high distress, and random networks were calculated using the Brain Connectivity Toolbox in Matlab (Rubinov and Sporns, 2010). The average characteristic path length of each group was calculated as the mean of the characteristic path lengths across all epochs. Similarly, the average clustering coefficient of each group was calculated as the mean clustering coefficients across all epochs. The small-worldness was calculated for the functional network in each epoch in the overlapping and non-overlapping sliding window conditions. The average small-worldness was calculated as the average of the measure across all epochs. The variance of the small-worldness was also calculated across the 163 and 55 epochs in the overlapping and non-overlapping window conditions in the controls, low distress, and high distress groups. The

Table 2
List of Brodmann areas used in the study.

Brodmann areas	Abbreviation	Name of the Brodmann area
BA01	S1	Primary somatosensory cortex
BA02	S2	Secondary somatosensory cortex
BA03	S3	Tertiary somatosensory cortex
BA04	M1	Primary motor cortex
BA05	SPS	Superior parietal sulcus
BA06	SMA	Supplementary motor area
BA07	SPG	Superior parietal gyrus
BA08	Pre-SMA	Pre-supplementary motor area
BA09	DLPFC	Dorsolateral prefrontal cortex
BA10	FPC	Fronto-parietal cortex
BA11	OFC	Orbital frontal cortex
BA13	Insula	Insula
BA17	V1	Primary visual cortex
BA18	V2	Secondary visual cortex
BA19	Cuneus	Cuneus
BA20	ITG	Inferior temporal gyrus
BA21	MTG	Medial temporal gyrus
BA22	STG	Superior temporal gyrus
BA23	PCC1	Posterior cingulate cortex1
BA24	dACC	Dorsal anterior cingulate cortex
BA25	sgACC	Subgenual anterior cingulate cortex
BA27	PHC1	Parahippocampal gyrus1
BA28	HIP1	Hippocampal area1
BA29	RSC1	Retrosplenial cortex1
BA30	RSC2	Retrosplenial cortex2
BA31	PCC2	Posterior cingulate cortex2
BA32	prACC	Pregenual anterior cingulate cortex
BA33	rACC	Rostral anterior cingulate cortex
BA34	HIP	Hippocampus
BA35	HIP2	Hippocampal area2
BA36	PHC2	Parahippocampal gyrus2
BA37	OTC	Occipital-temporal cortex
BA38	TP	Temporal pole
BA39	AG	Angular gyrus
BA40	IPS	Intra-parietal sulcus
BA41	A1	Primary auditory cortex
BA42	A2	Secondary auditory cortex
BA43	PCG	Postcentral gyrus
BA44	OPCG	Opercular part of inferior frontal gyrus
BA45	IFG	Inferior frontal gyrus
BA46	MPFC	Medial prefrontal cortex
BA47	VLPFC	Ventro-lateral prefrontal cortex

average functional connectivity strength at the network and connection level and the average small-worldness parameter are considered a measure of static connectivity. The variance in functional connectivity strength at the network and connection level and small-worldness parameter are considered measures of dynamic connectivity.

2.8. Probability of occurrence of a transient network configuration

In order to understand in detail how network configurations changed over time, we assumed that the brain could assume three possible configurations – small world, lattice, and random topology – at any given point of time. If the value is closer to 1, the network is said to be small-worlded. In order to arrive at the range of possible values that correspond to the range of small-world configurations, we derived the values of small-worldness corresponding to $+1.65$ and -1.65 Z-score (95% confidence interval) using the formula

$$\text{Range of small} - \text{worldness} = \frac{(\pm 1.65 * \sigma)}{\mu}$$

where, σ = standard deviation of the small-worldness parameter of the control group, μ = mean of the small-worldness parameter of the control group.

All values of small-worldness in the control, low distress, and high distress groups over the 163 epochs in the overlapping window, and 55 epochs in the non-overlapping window, were separated into small-world, random, and lattice configurations. The values in the three groups that lay between the upper and lower limit values of the small-world range were considered small-world configuration; values that were greater than the upper limit of the range were considered random configuration, and all the values below the lower limit of the range were considered lattice configuration. The number of occurrences of small-world, lattice, and random configurations in each frequency band was summed for each window condition. The probability that the system would be present in the small-world, lattice, or random configuration(state) was calculated by diving the total number of occurrences taken in the two alpha frequency bands by the total number of epochs in each window condition (326 for overlapping and 110 for non-overlapping windows).

2.9. Correlation with behavioral data

The network level measures of metastability i.e. the variance in functional connectivity strength in the low and high distress tinnitus groups were partially-correlated with the Tinnitus Questionnaire controlling for age, duration of tinnitus, and rating on the visual analog scale for loudness – a numeric scale where patients rate their loudness on a 10 cm scale and mean hearing loss. The hypothesis for the correlation analysis will depend on the results of the Bartlett test for variance. If there was a significant change in correlation coefficient, the amount of change in steepness of the slopes of the partial correlation between the variance and TQ score were compared between the low and high distress groups.

2.10. Statistical methods

2.10.1. Average functional connectivity

The average connectivity strength across the 163 sliding windows and 55 non-sliding windows was calculated in the low and high distress tinnitus and control groups in each frequency band. The average connectivity strength at the network level between the three groups in the two frequency bands ($3 * 2 = 6$ comparisons) were compared using an independent t-test assuming unequal variance corrected for multiple comparison at $p < .008$ (approximately .05/6). Further, an independent t-test assuming unequal variances was applied to compare the average connectivity strength between pairs of Brodmann areas across the time windows between the three groups at the different frequency bands. The comparisons were corrected for multiple comparisons using Bonferroni correction accounting for the number of connections ($83 * 84/2 = 3486$) in the network, number of groups (3) and the number of frequency bands (2) ($p < .000002$) ($.05/(3486 * 2 * 3)$).

2.10.2. Average graph parameters

The average characteristic path length, cluster coefficient, and small-world parameter of the low and high distress tinnitus groups and the control group in the in the two frequency bands were compared using an independent t-test assuming unequal variance corrected for multiple comparison at $p < .008$. This comparison was performed in both the overlapping and non-overlapping window condition.

2.10.3. Temporal variance of connectivity and small-world parameter

A Bartlett-test was applied to compare the variance in connectivity strength of the network, small-worldness of the network, and connectivity strength of each pairwise connection between low and high distress tinnitus and control groups, both in the overlapping and non-overlapping sliding window conditions. The Bartlett-test was also corrected for multiple comparisons using Bonferroni correction accounting for the number of frequencies and connections. In order to account for multiple comparisons, a $p < .008$ was used at the network level and $p < .000002$ at the connection level.

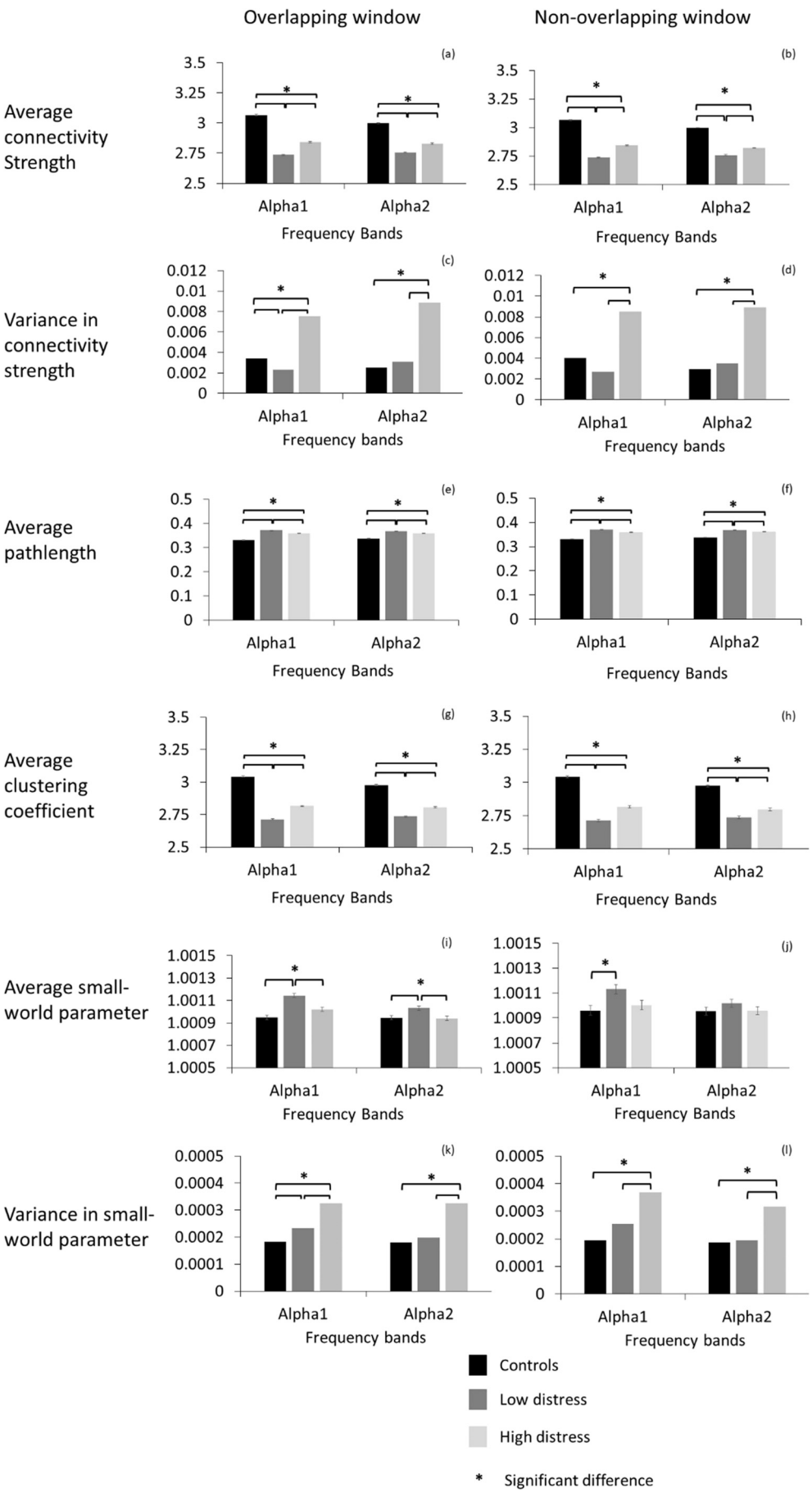

(caption on next page)

Fig. 2. Network level measures in the two sliding window conditions – (a) and (b) display the network level measures of average connectivity strength; (c) and (d) display the network level measures of variance in connectivity strength; (e) and (f) display the average characteristic path length; (g) and (h) display the average clustering coefficient; (i) and (j) display the average small-world parameter and (k) and (l) display the variance in the small-world parameter in the overlapping and non-overlapping windows respectively in the alpha1 and alpha2 frequency bands in controls (black bars), low distress tinnitus patients (dark grey bars) and high distress tinnitus patients (light grey bars). The error bars represent standard error bars.

2.10.4. Probability of occurrence of a transient network configuration

The overall association between the 3 groups and probability of occurrence of the 3 possible configurations, in the overlapping and non-overlapping window condition, in the two frequency bands taken together was analyzed using a 3 × 3 chi-square contingency table. In the presence of a significant group × topology interaction, a comparison of the probability of occurrence of topologies between individual groups was performed using individual chi-square tests in the overlapping and non-overlapping windows.

3. Results

3.1. Average connectivity

Changes in average connectivity over all the epochs in both the sliding and non-sliding window condition followed very similar patterns (Fig. 2a, b). Within the overlapping window condition, in the alpha1 frequency band, the connectivity strength of the control group was significantly higher than both the low ($t = 55.76$, $p < .001$) and high distress ($t = 27.43$, $p < .001$) tinnitus groups. The connectivity strength of the high distress tinnitus group was significantly greater than the low distress tinnitus group ($t = 13.71$, $p < .001$). In the alpha2 frequency band, the connectivity strength of the control group was significantly higher than both the low ($t = 41.23$, $p < .001$) and high distress tinnitus ($t = 20.26$, $p < .001$) groups. The connectivity strength of the high distress tinnitus group was significantly greater than the low distress tinnitus group ($t = 8.56$, $p < .001$).

Similarly, within the non-overlapping window condition, in the alpha1 frequency band, the connectivity strength of the control group was significantly higher than both the low ($t = 29.69$, $p < .001$) and high distress ($t = 14.68$, $p < .001$) tinnitus groups. The connectivity strength of the high distress tinnitus group was significantly greater than the low distress tinnitus group ($t = 7.51$, $p < .001$). In the alpha2 frequency band, the connectivity strength of the control group was significantly higher than both the low ($t = 22.02$, $p < .001$) and high distress tinnitus ($t = 12.00$, $p < .001$) groups. The connectivity strength of the high distress tinnitus group was significantly greater than the low distress tinnitus group ($t = 4.16$, $p < .001$).

A similar pattern was observed at the connection level as well. The connectivity strength of most connections in the control group was significantly greater than in the low and high distress tinnitus groups. The connectivity strengths of most of the connections in the high distress tinnitus group were significantly greater than those in the low distress tinnitus group. This was observed in both the overlapping and non-overlapping window conditions in both the frequency bands (Fig. 3).

3.2. Variance in functional connectivity (metastability)

At the network level, changes in variance of functional connectivity from the overlapping and non-overlapping window conditions followed a similar pattern (Fig. 2c, d). In the overlapping window condition, in the alpha1 band, the variance in functional connectivity of the high distress group was significantly higher than the low distress ($F = 53.07$, $p < .001$) and the control groups ($F = 24.06$, $p < .001$). The variance in functional connectivity of the control group was higher than the low distress tinnitus group ($F = 6.31$, $p = .012$). In the alpha2 frequency band, the variance in functional connectivity of the high distress group was significantly higher than the low distress ($F = 42.79$, $p < .001$) and the control group ($F = 59.19$, $p < .001$), but the variance in functional connectivity of the control group was not significantly different from the low distress group ($F = 1.54$, $p = .214$).

From non-overlapping window condition, in the alpha1 band, the variance in functional connectivity of the high distress group was significantly higher than the low distress ($F = 16.59$, $p < .001$) and the control group ($F = 7.25$, $p = .007$). The variance in functional connectivity of the control group was not significantly different from the low distress tinnitus group ($F = 2.11$, $p = .147$). In the alpha2 frequency band, the variance in functional connectivity of the high distress group was significantly higher than the low distress ($F = 11.16$, $p < .001$) and the control group ($F = 15.64$, $p < .001$), but the variance in functional connectivity of the control group was not significantly different from the low distress group ($F = 0.43$, $p = .513$).

A similar pattern was observed at the connection level in both the alpha1 and alpha2 bands of the overlapping and non-overlapping window conditions. The variance of the connectivity strength of most of the connections in the controls and low distress groups were not significantly different from each other. However, the variance in connectivity strength of most of the connections from the high distress group was significantly greater than that of the low distress and control groups (Fig. 4).

3.3. Average characteristic path length

Changes in average characteristic path length over all the epochs, in both the sliding and non-sliding window condition, followed very similar patterns (Fig. 2e, f). Within the overlapping window condition, in the alpha1 frequency band, the average characteristic path length of the control group was significantly lower than both the low ($t = 57.85$, $p < .001$) and high distress ($t = 29.37$, $p < .001$) tinnitus groups. The average characteristic path length of the high distress tinnitus group was significantly lower than the low distress tinnitus group ($t = 12.42$, $p < .001$). In the alpha2 frequency band, the average characteristic path length of the control group was significantly lower than both the low ($t = 41.47$, $p < .001$) and high distress ($t = 21.51$, $p < .001$) tinnitus groups. The average characteristic path length of the high distress tinnitus group was significantly lower than the low distress tinnitus group ($t = 7.42$, $p < .001$).

Similarly, within the non-overlapping window condition, in the alpha1 frequency band, the average characteristic path length of the control group was significantly lower than both the low ($t = 31.20$, $p < .001$) and high distress ($t = 15.73$, $p < .001$) tinnitus groups. The average characteristic path length of the high distress tinnitus group was significantly lower than the low distress tinnitus group ($t = 6.75$, $p < .001$). In the alpha2 frequency band, the average characteristic path length of the control group was significantly lower than both the low ($t = 21.95$, $p < .001$) and high distress ($t = 12.71$, $p < .001$) tinnitus groups. The average characteristic path length of the high distress tinnitus group was significantly lower than the low distress tinnitus group ($t = 3.36$, $p = .001$).

3.4. Average clustering coefficient

Changes in the average clustering coefficient over all epochs, in both the sliding and non-sliding window condition, followed very similar patterns (Fig. 2g, h). Within the overlapping window condition, in the alpha1 frequency band, the average clustering coefficient of the control group was significantly higher than both the low ($t = 56.00$, $p < .001$) and high distress ($t = 28.00$, $p < .001$) tinnitus groups. The average clustering coefficient of the high distress tinnitus group was

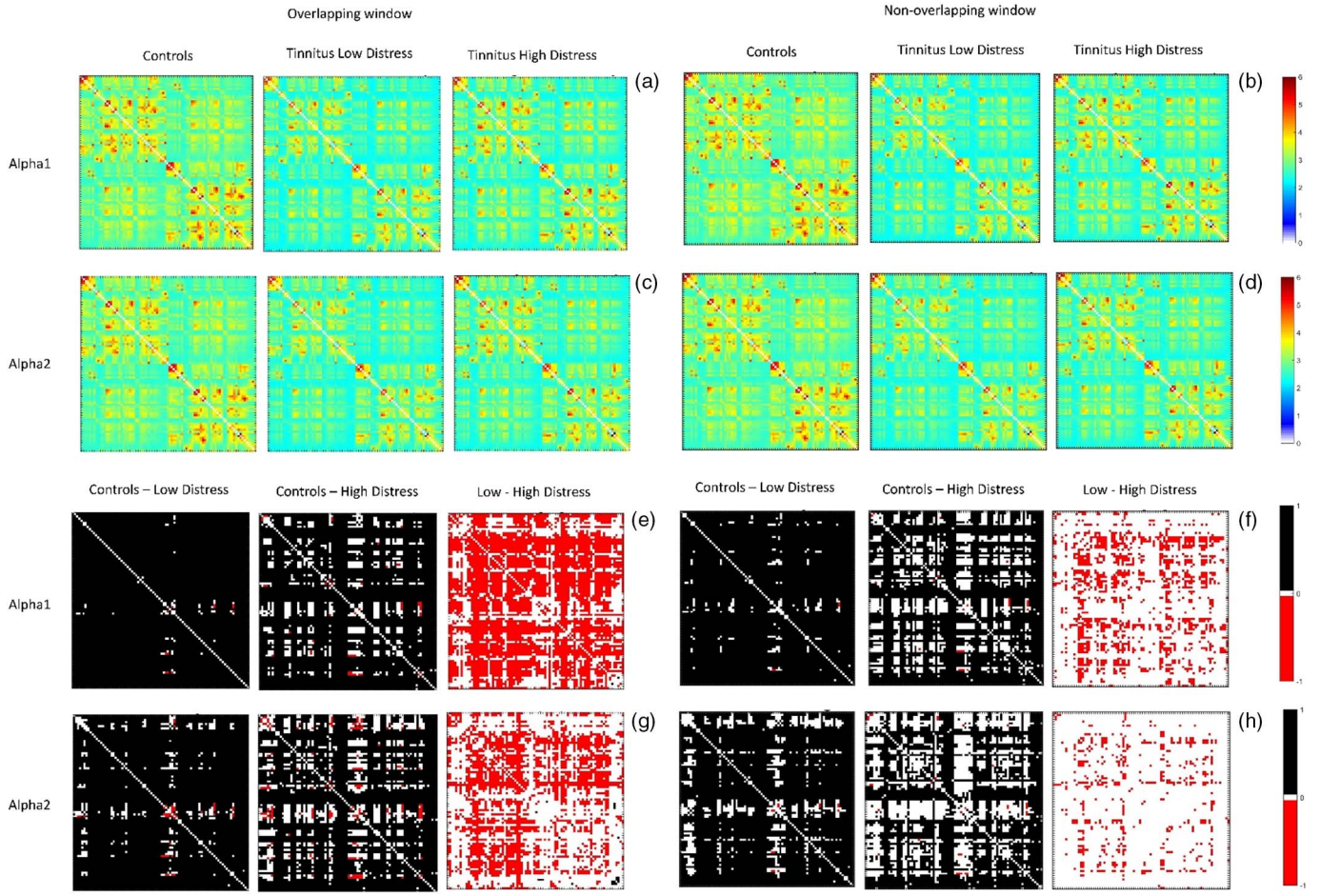

Fig. 3. Average connectivity strength of an edge and difference in connectivity strength between the three groups in the overlapping and non-overlapping sliding window condition. (a) and (b) show the average functional connectivity strength in the controls (right panel), low distress (middle panel) and high distress (left panel) tinnitus patients in the alpha1 frequency band; (c) and (d) show the same in the alpha2 frequency band in the overlapping and non-overlapping window condition respectively. (e) and (f) show the difference in connectivity strength between the controls and low distress group (right panel), controls and high distress group (middle panel) and low and high distress group (left panel) in the alpha1 frequency band; (g) and (h) show the same in the alpha2 frequency band in the overlapping and non-overlapping window conditions respectively. In a generic A–B difference in functional connectivity strength, connections in black show significantly greater connectivity strength in group A, connections in red show significantly greater connectivity strength in group B and connections in white are those connections that are not significantly different from one another. (For interpretation of the references to colour in this figure legend, the reader is referred to the web version of this article.)

significantly greater than the low distress tinnitus group ($t = 13.35$, $p < .001$). In the alpha2 frequency band, the average clustering coefficient of the control group was significantly higher than both the low ($t = 41.34$, $p < .001$) and high distress tinnitus ($t = 20.68$, $p < .001$) groups. The connectivity strength of the high distress tinnitus group was significantly greater than the low distress tinnitus group ($t = 8.28$, $p < .001$).

Similarly, within the non-overlapping window condition, in the alpha1 frequency band, the average clustering coefficient of the control group was significantly higher than both the low ($t = 29.87$, $p < .001$) and high distress ($t = 14.98$, $p < .001$) tinnitus groups. The average clustering coefficient of the high distress tinnitus group was significantly greater than the low distress tinnitus group ($t = 7.31$, $p < .001$). In the alpha2 frequency band, the clustering coefficient of the control group was significantly higher than both the low ($t = 22.00$, $p < .001$) and high distress tinnitus ($t = 12.23$, $p < .001$) groups. The average clustering coefficient of the high distress tinnitus group was significantly greater than the low distress tinnitus group ($t = 3.96$, $p < .001$).

3.5. Average small-world parameter

Changes in the average small-world parameter over all epochs, in both the sliding and non-sliding window condition, followed very similar patterns (Fig. 2i, j). Within the overlapping window condition, in the alpha1 frequency band, the average small-world parameter of the control group was significantly lower than the low distress group ($t = 8.44$, $p < .001$) and not significantly different from the high distress group ($t = 2.48$, $p = .014$). The average small-world parameter of the high distress tinnitus group was significantly lower than the low distress tinnitus group ($t = 3.94$, $p < .001$). In the alpha2 frequency band, the average small-world parameter of the control group was significantly lower than the low distress group ($t = 4.18$, $p < .001$) and not significantly different from the high distress group ($t = 0.19$, $p = .848$). The small-world parameter of the high distress tinnitus group was significantly lower than the low distress tinnitus group ($t = 3.12$, $p = .002$).

However, within the non-overlapping window condition, in the alpha1 frequency band, the average small-world parameter of the control group was significantly lower than the low distress group ($t = 3.97$, $p < .001$) and not significantly different from the high distress group ($t = 0.76$, $p = .452$). The average small-world parameter of the high distress tinnitus group was also not significantly different from the low distress tinnitus group ($t = 2.15$, $p = .035$). In the alpha2 frequency band, there were no significant differences in the average small-world parameter in between the control group and low ($t = 1.78$,

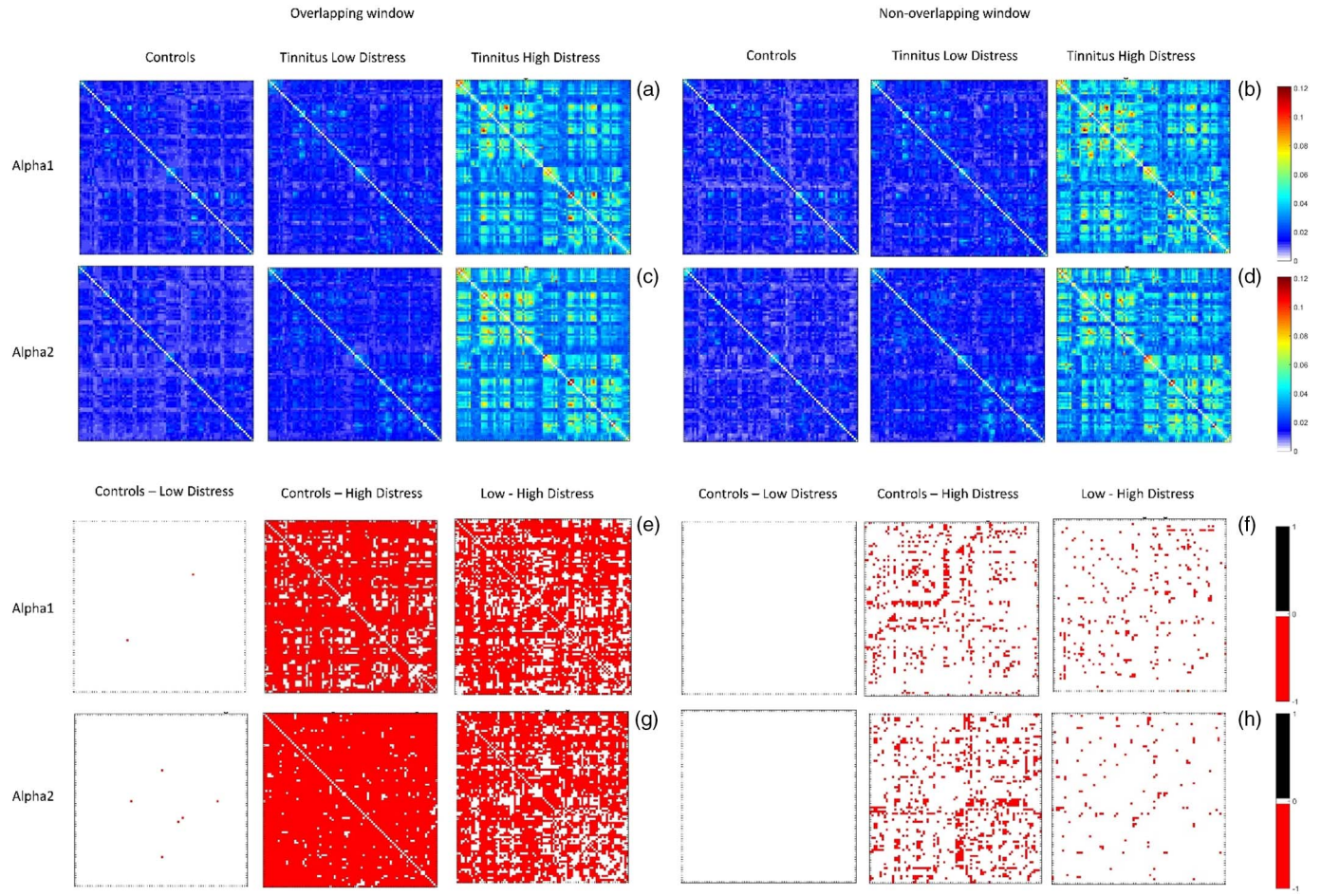

Fig. 4. Variance in functional connectivity strength of an edge and difference in variance between the three groups in the overlapping and non-overlapping sliding window condition. (a) and (b) show the variance in functional connectivity strength in the controls (right panel), low distress (middle panel) and high distress (left panel) tinnitus patients in the alpha1 frequency band; (c) and (d) show the same in the alpha2 frequency band in the overlapping and non-overlapping window condition respectively. (e) and (f) show the difference in variance between the controls and low distress group (right panel), controls and high distress group (middle panel) and low and high distress group (left panel) in the alpha1 frequency band; (g) and (h) show the same in the alpha2 frequency band in the overlapping and non-overlapping window conditions respectively. In a generic A–B difference in variance in functional connectivity strength, connections in black show significantly greater variance in connectivity strength in group A, connections in red show significantly greater variance in connectivity strength in group B and connections in white are those connections that are not significantly different from one another. (For interpretation of the references to colour in this figure legend, the reader is referred to the web version of this article.)

$p = .078$) and high distress ($t = 0.09$, $p = .931$) tinnitus group, or between the low and high distress tinnitus groups ($t = 1.21$, $p = .230$).

3.6. Variance of small-world parameter

Changes in variance of the small-world parameter in the overlapping and non-overlapping window conditions followed a similar pattern (Fig. 2k, l). Within the overlapping window condition, in the alpha1 frequency band, the variance of the small-world parameter in the control group was significantly lower than that of the low distress ($F = 9.57$, $p = .002$) and high distress tinnitus group ($F = 50.85$, $p < .001$) and the variance of the small-world parameter of the low distress group was significantly lower than that of the high distress tinnitus group ($F = 17.42$, $p < .001$). In the alpha 2 frequency band, the variance of the small world parameter in the control group was significantly lower than the high distress group ($F = 53.33$, $p < .001$) but not from the low distress group ($F = 1.40$, $p = .236$). The variance of the small-world parameter in the low distress group was significantly lower than the high distress group ($F = 38.39$, $p < .001$).

Within the non-overlapping window condition, in the alpha1 frequency band, the variance of the small-world parameter of the control group was significantly lower than that of the high distress tinnitus group ($F = 20.22$, $p < .001$), but not the low distress group ($F = 3.71$, $p = .054$), and the variance of the small-world parameter in the low distress group was significantly lower than that of the high distress tinnitus group ($F = 7.14$, $p = .008$). In the alpha 2 frequency band, the variance of the small world parameter in the control group was significantly lower than the high distress group ($F = 13.62$, $p < .001$) but not from the low distress group ($F = 0.01$, $p = .918$). The variance of the small-world parameter in the high distress group was significantly greater than the low distress group ($F = 12.92$, $p < .001$).

A summary of the results of static and dynamic connectivity common to both the frequency bands and the two sliding window conditions are shown in Table 3.

3.7. Probability of occurrence of a transient network configuration

In the overlapping ($\chi^2 = 106.97$, $p < .001$) and non-overlapping ($\chi^2 = 23.25$, $p < .001$) window conditions, we observed a significant interaction between group and topology where the association between group and topology were significantly different for the different groups. Changes in average connectivity over all the epochs in both the sliding and non-sliding window condition followed very similar patterns (Fig. 5a, b). In the overlapping window condition, the probability of occurrence of the small-world topology was significantly lower in the low distress ($\chi^2 = 23.62$, $p < .001$) and high distress ($\chi^2 = 62.20$,

Table 3
Summary of results of average and dynamic functional connectivity common to both frequency bands in the overlapping and non-overlapping window conditions.

Static and dynamic measures	Summary of results
Average connectivity strength	Controls > High distress > Low distress
Average cluster coefficient	Controls > High distress > Low distress
Average path length	Low distress > High distress > Controls
Average small-world parameter	Low distress > High distress ~ Controls
Variance in functional connectivity strength	High distress > Low distress = Controls
Variance in small-world parameter	High distress > Low distress = Controls

$p < .001$) tinnitus group as compared to the control group. The probability of occurrence of the small-world topology in the high distress tinnitus group was significantly lower than the low distress group tinnitus group ($\chi^2 = 10.46$, $p = .001$). The probability of occurrence of the random topology was significantly higher in the low ($\chi^2 = 39.95$, $p < .001$) and high distress tinnitus group ($\chi^2 = 27.90$, $p < .001$) compared to the control group. However, no significant difference was observed in the difference in probability of occurrence of the random topology between low distress group and high distress tinnitus group ($\chi^2 = 1.31$, $p = .253$). The probability of occurrence of the lattice topology was significantly higher in the high distress tinnitus group compared to the low distress tinnitus ($\chi^2 = 47.20$, $p < .001$) and control groups ($\chi^2 = 26.24$, $p < .001$). The probability of occurrence of the lattice topology was significantly lower in the low distress tinnitus group compared to the control group ($\chi^2 = 5.73$, $p = .017$).

However, in the non-overlapping window condition, the probability of occurrence of the small-world topology was significantly lower in the high distress tinnitus group ($\chi^2 = 10.91$, $p = .001$) compared to the control group, but no significant difference was found between the low distress tinnitus group and the control group ($\chi^2 = 1.95$, $p = .163$). The difference in probability of occurrence of the small-world topology in the high distress and the low distress tinnitus group was marginally significant ($\chi^2 = 3.82$, $p = .051$). The probability of occurrence of the random topology was significantly higher in the low distress tinnitus group compared to the control group ($\chi^2 = 5.24$, $p = .022$). However, no significant difference was observed in the difference in probability of occurrence of the random topology between low distress group and high distress tinnitus group ($\chi^2 = 0.27$, $p = .604$) and the high distress group and control group ($\chi^2 = 3.20$, $p = .074$). The probability of occurrence of the lattice topology was significantly higher in the high distress tinnitus group compared to the low distress tinnitus ($\chi^2 = 14.01$, $p < .001$) and control groups ($\chi^2 = 6.71$, $p = .01$). However, no significant difference was observed between the probability of occurrence of the lattice topology between the low distress tinnitus group compared to the control group ($\chi^2 = 2.06$, $p = .15$). The difference in results between the overlapping and non-overlapping window conditions, in spite of similar magnitude of difference in the two conditions between the different groups, may be attributed to the reduced degrees of freedom in the non-overlapping window condition ($df = 109$) compared to the overlapping window condition ($df = 325$).

3.8. Correlation of behavioral measures with variance of functional connectivity

We hypothesize that the results of the correlation of the variance in functional connectivity with tinnitus distress will follow the results of the Bartelett test for changes in variance. From the Bartlett test, we observe that in both the overlapping and non-overlapping window conditions, there was no significant change in variance observed for the low distress group, but a significant increase in variance for the high distress group. Thus, we hypothesize based on these results that there will be no significant correlation of tinnitus distress and variance in functional connectivity in the low distress group, but a significant positive correlation between tinnitus distress and variance in functional connectivity in the high distress group. Thus, a one-tailed correlation was performed between tinnitus distress (TQ score) and the variance in functional connectivity in the two alpha frequency bands. The one-tailed p-value was corrected for multiple comparison for the two frequency bands $p < .025$ (.05/2).

In the overlapping window condition, we observed no significant correlation between variance and TQ score in the alpha1 ($r = -0.11$, $p = .262$) and alpha2 ($r = -0.17$, $p = .155$) frequency bands in the low distress group. However, we observed a significant positive correlation between variance and TQ score in the alpha1 frequency band ($r = 0.60$, $p = .021$) and not in the alpha2 frequency band ($r = 0.55$, $p = .032$) (Fig. 6a).

Similarly, in the non-overlapping window condition, we observed no significant correlation between variance and TQ score in the alpha1 ($r = -0.08$, $p = .314$) and alpha2 ($r = -0.21$, $p = .112$) frequency bands in the low distress group. However, we observed a significant positive correlation between variance and TQ score in the alpha1 frequency band ($r = 0.58$, $p = .023$) and not in the alpha2 frequency band ($r = 0.50$, $p = .049$) (Fig. 6c, d). Further, the change in the steepness of the partial correlation between the variance in functional connectivity and TQ score was significantly increased in the high distress compared

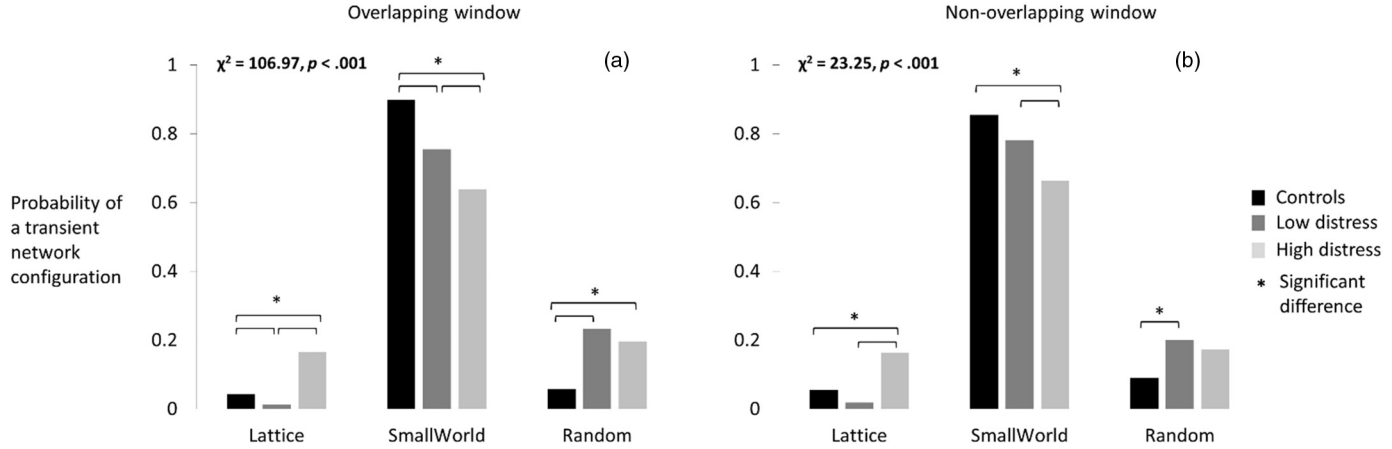

Fig. 5. Probability of transient network configurations in the overlapping and non-overlapping sliding window conditions. (a) and (b) show the comparison of the probability of the occurrence of a transient network configuration i.e. the small-world, lattice and random topologies over the 3 min of recording in the controls, low distress and high distress tinnitus groups in the overlapping and non-overlapping window conditions respectively.

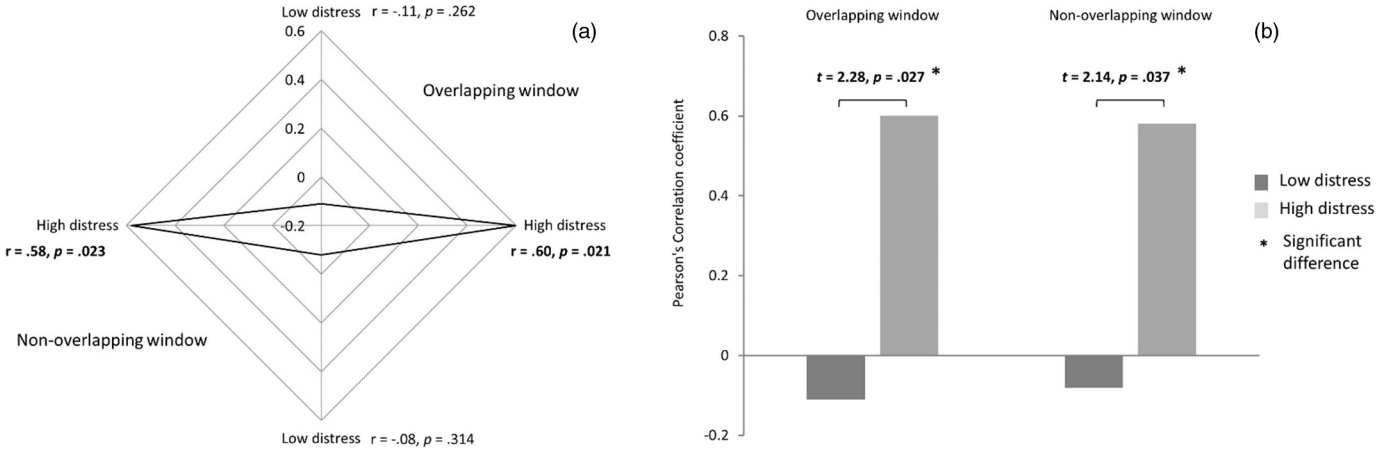

Fig. 6. Partial correlations of variance in functional connectivity with TQ score in (a) low and high distress tinnitus group in the overlapping and non-overlapping sliding window conditions in the alpha1 frequency band. (b) Shows significant difference in the partial correlations of TQ score with variance in functional connectivity between the low and high distress groups in the overlapping and non-overlapping window conditions in the alpha1 frequency band.

to the low distress tinnitus group in the alpha1 frequency band in the overlapping ($t = 2.28$, $p = .027$) and non-overlapping ($t = 2.14$, $p = .037$) window conditions (Fig. 6b).

4. Discussion

The current study investigates the relationship between chronic distress in the presence of pathology, metastability, and the balance between functional integration and segregation. This was investigated by examining the overall and transient changes in functional connectivity and network topology over time (i.e. recording) using resting state EEG. From the results of the mean functional connectivity across 3 min of the recording, we observed an overall decrease in transfer of information between long distance and local connections, in both the low distress and high distress groups compared to the control group. This is characterized by an increase in average path length and decrease in average clustering coefficient. These results are consistent with our previous findings where we examine the changes in graph theoretical parameters calculated from the static functional connectivity matrix in control and tinnitus groups (Mohan et al., 2016b). However, we observed an overall increase in transfer of information over long distance and local connections in the high distress group compared to the low distress group. This is characterized by a decrease in average path length and increase in average clustering coefficient. Decrease in average connectivity strength in the low and high distress tinnitus group compared to the control group, and increase in connectivity strength of the high distress group compared to the low distress group seems to be spread out across the brain. Such an increase in a disease state (high distress), termed “hyperconnectivity”, has shown to be evident in several disorders such as depression, autism, and schizophrenia, and has been hypothesized as a compensatory mechanism of the brain to overcome loss of function (Berman et al., 2011; Hillary and Grafman, 2017; Supekar et al., 2013; Whitfield-Gabrieli et al., 2009). These changes in measures of mean functional integration and segregation are reflected in changes in network topology. On average, we observe that the functional network of the low distress group shifts to a more random topology compared to the control network, and there is seemingly no difference in the network topology between the high distress tinnitus and control groups. From this we may conclude that in the high distress group, although there is a decrease in local and long-distance connectivity, there seems to be an overall balance between network integration and segregation.

However, by comparing the transient changes in functional connectivity strength and network topology, we observed no significant difference in the fluctuation in functional connectivity and network topology between the controls and low distress groups, but a significant increase in the high distress group. Once again, these changes seem to reflect across most connections in the whole-brain network in the high distress group. This characterizes an increase in metastability of the brain, or increased fluctuation between transient stable states in the high distress group, accompanied by large fluctuations in the balance between network integration and segregation (Deco and Kringelbach, 2016; Shanahan, 2010; Váša et al., 2015).

In order to better interpret the changes in the mean and variance of the network topology, and understand the concept of changes in metastability from a conceptual standpoint, let us assume that at any given epoch the network could broadly assume one of three configurations – small-world, lattice, and random – characterized by the small-world parameter, and let each of these configurations correspond to a transient state. When the small world parameter is close to 1, it is proposed that the network topology is perfectly balanced between functional integration and segregation; when it is > 1, then functional integration is greater than functional segregation and the network starts shifting to a more random topology. When it is < 1, then functional segregation is greater than functional integration and the network starts shifting to a lattice topology. Thus, from the probability of a network configuration occurring across 3 min of continuous recording, we observed that the control network is mostly present in the small-world state and equally fluctuates between lattice and random states. In the low-distress group, the probability that the network is present in the small-world state was between that of the control and high distress group and fluctuates more often to the random state than to the lattice state. In the high distress group, the probability that the network is present in the small-world state was significantly lower than both the controls and low distress group. Although the frequency of fluctuation to the random state was similar to the low distress group, the network in the high distress group fluctuates with nearly equal probability to the lattice state as well. From these observations, we clearly see that the shift of the average topology of the low distress group to a more random topology may be attributed to the increase in probability of the system's existence in the random state. Further, the paradoxical “balance” in the average network topology of the high distress group may be attributed to the similarity in pattern of fluctuation between the controls and high distress groups. However, the significantly higher probability of fluctuation to the lattice and random topology of the high distress groups, compared to the low distress and control groups, fits together with the increase in metastability in the high distress group. Distress is also attributed to a hyper-salience in the brain (De Ridder et al., 2014). Salience directly refers to top-down goal related attention which possibly results in hyper-focusing on the disorder (Mohan and Vanneste, 2017; White

et al., 2010). Thus, the increase in metastability could be a maladaptive compensatory mechanism of the brain to look for information in order to reduce the hyper-salience in highly distressed individuals. In other words, the brain possibly increases its fluctuation between multiple, transient metastable states and increases its degrees of freedom by increasing its range of network configurations to compensate for the hyper-salience in highly distressed individuals.

The relationship between changes in fluctuation between transient network configurations and the resilience of the brain could be explained by Selye's General Adaptation Syndrome (Campbell et al., 2013; Selye, 1946). According to Selye, chronic stress has two types of effects on the body, and in this case, the brain. In the resistance phase, the brain/body is in a state of high physiological arousal and presents an adaptive response to the stressor, thus actively resisting the negative effects of the presence of the stressor (Campbell et al., 2013). This resistance can also be viewed as the resilience of the brain/body to changes in different parameters that may be affected by the stressor. In the exhaustion phase, there is a catastrophic breakdown of the brain's adaptive response and depletion of reserves, and it succumbs to the negative effects of the stressor and results in a chronic illness (Campbell et al., 2013). In the current study, the perception of a phantom sound acts as the stressor in both the low and high distress tinnitus groups. However, the difference in the amount of distress caused by the stressor in the two groups may be attributed to how the brain responds to the stressor per Selye's theory. In the low distress group, although there is an overall shift to a more random topology, the transient fluctuations around this average topology remain unchanged. This is also evident in the preservation of variance in both functional connectivity and small-world parameters between control and low distress groups. This preservation of fluctuation around this new topology may be attributed to the brain's adaptive response to resist the negative effects of the stressor. Further, the absence of a correlation between variance in functional connectivity and the amount of distress perceived in the low distress groups demonstrates the resilience of this state to temporal changes in connectivity, or external factors that may influence the psychological distress component.

However, in the high distress group we observe that the variance in functional connectivity and the fluctuations around its average network topology are both significantly higher than that of the low distress group. Further, we observe a significant positive correlation between the variance in functional connectivity and the amount of perceived distress. This could mean that in the high distress group, the brain enters the exhaustion phase where there is a catastrophic breakdown of its resistance to the stressor and the network becomes less resilient. Thus, the increase in fluctuation of the average network topology, going from order to randomness in highly distressed patients, exhibits an increase in fluctuation between transient metastable states.

Thus, in the current study we show that the presence of a stressor, such as tinnitus, can induce a change in the overall network topology and shift the normal, small-world network to a more random network, characterized by a decrease in long distance and local connectivity in the alpha bands. This agrees with the hypothesis that stress changes the normal healthy state of the brain to a lower utility state (Oken et al., 2015). Per the results of the current study, the stability and resilience of this state depends on the amount of distress perceived by the patients. In patients with low distress, the new state is resilient to temporal changes in functional connectivity and changes in network topology. However, in patients with high distress, this state becomes more sensitive to temporal variations in functional connectivity, leading to an increase in fluctuation of network topology. This increases the degrees of freedom and leads to a paradoxical stability of the current state characterized by increased inter- and intra-community communication. These results are complementary to our findings from static functional connectivity. In our previous studies, we showed that the tinnitus network shifts from the usual small world topology to a random or lattice topology in a frequency dependent way (Mohan et al., 2016b). Further, these shifts were characterized by either a change in connectivity strength, change in important regions controlling information flow or a combination of both (Mohan et al., 2016a). Specifically, in the alpha frequency bands, we observed that the shift to a more lattice topology was engineered by changes in hubs and connectivity strength (Mohan et al., 2016a,b). In the current study, where our data overlaps with these previous studies, we observe that this shift changes temporally and depends on the amount of distress perceived by the patients. Patients with low distress present an increased probability of shifting to a random topology, whereas the high distress patients sway from a lattice to random with almost equal probability. Further, analogous to static functional connectivity, these temporal shifts in network topology depend on the changes in dynamic functional connectivity.

The current study is one of the first studies to investigate the relationship between transient changes in network topology and how it may relate to chronic distress in the presence of a pathological stressor. Thus, the current study presents a dynamic neural marker to chronic distress and the resilience of the brain to chronic distress. Since distress is a domain-general symptom, the neural marker presented in this study may be a domain-general phenomenon generalizing to other chronic pathologies.

4.1. Limitations

The current study successfully investigates the temporal changes in functional connectivity, metastability and functional network topology in chronic distress in tinnitus patients, however with some limitations. Previous studies show that functional connectivity of the tinnitus group shows changes with hearing loss and differs between male and female. However, the tinnitus population in current study is not matched for hearing loss and sex ratio within the tinnitus group and with the control group and hence future studies replicating the same results with a more controlled population would be worthwhile. Second, the study uses a low-resolution source localization technique to identify 84 Brodmann areas. This limits the findings of the current technique only to cortical areas and the connections with mesolimbic structures have been shown to play a significant role may in modulating tinnitus distress. The replication of the current technique with high resolution techniques will help with not only confirming the results but investigating the dynamics of deeper subcortical structures.

5. Conclusion

The current study successfully investigates the changes in transient network dynamics and network topology in a disorder, such as tinnitus, that arouses a distress component. We observe that distress has a non-linear effect on the transient network dynamics and the network structure. Patients with low distress demonstrate a more random, yet resilient dynamics characterized by a preservation in fluctuation of transient stable states and network topology. However, high distress patients demonstrate an increase in fluctuation in transient stable states and network topology, characterizing a possible breakdown of the brain's adaptive response to the stressor (i.e., tinnitus). This paradoxically increases the number of degrees of freedom of the brain, and results in an undesired balance of the network topology in the diseased state. Such an undesired stability, due to the increase in fluctuation between transient states, may also be a maladaptive compensation to increase in salience in highly distressed individuals.

Supplementary data to this article can be found online at https://doi.org/10.1016/j.pnpbp.2018.01.025.

Conflict of interest

The authors declare no competing financial interests or any other conflict of interest.

Human rights ethics statement

This study was approved by the local ethical committee (Antwerp University Hospital) and was in accordance with the declaration of Helsinki. Collection of the data was under approval of IRB UZA OGA85. All patients gave a written informed consent.

Author contribution

AM: Data analysis and writing the manuscript.
SJA: Data analysis and manuscript preparation.
CVJ: Data analysis and manuscript preparation.
DDR: Data collection and writing the manuscript.
SV: Data collection and writing the manuscript.

Funding sources

No funding sources were involved in this study.

Data statement

The data remains with the Corresponding Author and maybe available on request.

References

Audiology, B.S.O., 2008. Recommended procedure:pure tone air and bone conduction threshold audiometry with and without masking and determination of uncomfortable loudness levels.
Bassett, D.S., Bullmore, E., 2006. Small-world brain networks. Neuroscientist 12, 512–523.
Berman, M.G., Peltier, S., Nee, D.E., Kross, E., Deldin, P.J., Jonides, J., 2011. Depression, rumination and the default network. Soc. Cogn. Affect. Neurosci. 6, 548–555.
Bloomfield, P., 2004. Fourier Analysis of Time Series: An Introduction. John Wiley & Sons.
Bullmore, E., Sporns, O., 2012. The economy of brain network organization. Nat. Rev. Neurosci. 13, 336–349.
Campbell, T.S., Johnson, J.A., Zernicke, K.A., 2013. General adaptation syndrome. In: Gellman, M.D., Turner, J.R. (Eds.), Encyclopedia of Behavioral Medicine. Springer New York, New York, NY, pp. 842–844.
Chen, Y.C., Xia, W., Chen, H., Feng, Y., Xu, J.J., Gu, J.P., ... Yin, X., 2017. Tinnitus distress is linked to enhanced resting-state functional connectivity from the limbic system to the auditory cortex. Hum. Brain Mapp. 38 (5), 2384–2397.
Congedo, M., 2002. EureKa! (Version 3.0) [Computer Software]. NovaTech EEG Inc., Knoxville, TN Freeware available at. www.NovaTechEEG.
Congedo, M., John, R.E., De Ridder, D., Prichep, L., Isenhart, R., 2010. On the "dependence" of "independent" group EEG sources; an EEG study on two large databases. Brain Topogr. 23, 134–138.
Córdova-Palomera, A., Kaufmann, T., Persson, K., Alnæs, D., Doan, N.T., Moberget, T., Lund, M.J., Barca, M.L., Engvig, A., Brækhus, A., 2017. Disrupted global metastability and static and dynamic brain connectivity across individuals in the Alzheimer's disease continuum. Sci. Rep. 7, 40268.
De Ridder, D., Vanneste, S., Congedo, M., 2011a. The distressed brain: a group blind source separation analysis on tinnitus. PLoS One 6, e24273.
De Ridder, D., Elgoyhen, A.B., Romo, R., Langguth, B., 2011b. Phantom percepts: tinnitus and pain as persisting aversive memory networks. Proc. Natl. Acad. Sci. 108, 8075–8080.
De Ridder, D., Vanneste, S., Weisz, N., Londero, A., Schlee, W., Elgoyhen, A.B., Langguth, B., 2014. An integrative model of auditory phantom perception: tinnitus as a unified percept of interacting separable subnetworks. Neurosci. Biobehav. Rev. 44, 16–32.
De Ridder, D., Congedo, M., Vanneste, S., 2015a. The neural correlates of subjectively perceived and passively matched loudness perception in auditory phantom perception. Brain Behav. 5, e00331.
De Ridder, D., Vanneste, S., Langguth, B., Llinas, R., 2015b. Thalamocortical dysrhythmia: a theoretical update in tinnitus. Front. Neurol. 6, 124.
Deco, G., Kringelbach, M.L., 2016. Metastability and coherence: extending the communication through coherence hypothesis using a whole-brain computational perspective. Trends Neurosci. 39, 125–135.
Dijkstra, E.W., 1959. A note on two problems in connexion with graphs. Numer. Math. 1, 269–271.
Fingelkurts, A.A., Fingelkurts, A.A., 2004. Making complexity simpler: multivariability and metastability in the brain. Int. J. Neurosci. 114, 843–862.
Fuchs, M., Kastner, J., Wagner, M., Hawes, S., Ebersole, J.S., 2002. A standardized boundary element method volume conductor model. Clin. Neurophysiol. 113 (5), 702–712.
Goebel, G., Hiller, W., 1994. The tinnitus questionnaire. A standard instrument for grading the degree of tinnitus. Results of a multicenter study with the tinnitus questionnaire. HNO 42.
Hillary, F.G., Grafman, J.H., 2017. Injured brains and adaptive networks: the benefits and costs of hyperconnectivity. Trends Cogn. Sci. 21 (5), 385–401.
Holling, C.S., 1973. Resilience and stability of ecological systems. Annu. Rev. Ecol. Syst. 4, 1–23.
Holling, C.S., 1996. Engineering resilience versus ecological resilience. Eng. Ecol. Constrain. 31, 32.
Humphries, M.D., Gurney, K., 2008. Network 'small-world-ness': a quantitative method for determining canonical network equivalence. PLoS One 3, e0002051.
Husain, F.T., Schmidt, S.A., 2014. Using resting state functional connectivity to unravel networks of tinnitus. Hear. Res. 307, 153–162.
Imperatori, C., Farina, B., Quintiliani, M.I., Onofri, A., Gattinara, P.C., Lepore, M., Gnoni, V., Mazzucchi, E., Contardi, A., Della Marca, G., 2014. Aberrant EEG functional connectivity and EEG power spectra in resting state post-traumatic stress disorder: a sLORETA study. Biol. Psychol. 102, 10–17.
Jastreboff, P.J., 1990. Phantom auditory perception (tinnitus): mechanisms of generation and perception. Neurosci. Res. 8, 221–254.
Jurcak, V., Tsuzuki, D., Dan, I., 2007. 10/20, 10/10, and 10/5 systems revisited: their validity as relative head-surface-based positioning systems. Neuroimage 34 (4), 1600–1611.
Kelso, J.S., Tognoli, E., 2006. Metastability in the brain. In: The 2006 IEEE International Joint Conference on Neural Network Proceedings. IEEE, pp. 363–368.
Kim, J.-Y., Kim, Y.-H., Lee, S., Seo, J.-H., Song, H.-J., Cho, J.H., Chang, Y., 2012. Alteration of functional connectivity in tinnitus brain revealed by resting-state fMRI? A pilot study. Int. J. Audiol. 51, 413–417.
Klimesch, W., 2012. Alpha-band oscillations, attention, and controlled access to stored information. Trends Cogn. Sci. 16, 606–617.
Klimesch, W., Sauseng, P., Hanslmayr, S., 2007. EEG alpha oscillations: the inhibition–timing hypothesis. Brain Res. Rev. 53, 63–88.
Kross, E., Egner, T., Ochsner, K., Hirsch, J., Downey, G., 2007. Neural dynamics of rejection sensitivity. J. Cogn. Neurosci. 19, 945–956.
Lancaster, J.L., Woldorff, M.G., Parsons, L.M., Liotti, M., Freitas, C.S., Rainey, L., ... Fox, P.T., 2000. Automated Talairach atlas labels for functional brain mapping. Hum. Brain Mapp. 10 (3), 120–131.
Landgrebe, M., Barta, W., Rosengarth, K., Frick, U., Hauser, S., Langguth, B., Rutschmann, R., Greenlee, M.W., Hajak, G., Eichhammer, P., 2008. Neuronal correlates of symptom formation in functional somatic syndromes: a fMRI study. NeuroImage 41, 1336–1344.
von Leupoldt, A., Sommer, T., Kegat, S., Baumann, H.J., Klose, H., Dahme, B., Büchel, C., 2009. Dyspnea and pain share emotion-related brain network. NeuroImage 48, 200–206.
Llinás, R.R., Ribary, U., Jeanmonod, D., Kronberg, E., Mitra, P.P., 1999. Thalamocortical dysrhythmia: a neurological and neuropsychiatric syndrome characterized by magnetoencephalography. Proc. Natl. Acad. Sci. 96, 15222–15227.
Maudoux, A., Lefebvre, P., Cabay, J.E., Demertzi, A., Vanhaudenhuyse, A., Laureys, S., Soddu, A., 2012. Connectivity graph analysis of the auditory resting state network in tinnitus. Brain Res. 1485, 10–21.
Mazziotta, J., Toga, A., Evans, A., Fox, P., Lancaster, J., Zilles, K., ... Holmes, C., 2001. A four-dimensional probabilistic atlas of the human brain. J. Am. Med. Inform. Assoc. 8 (5), 401–430.
Meeus, O., Blaivie, C., Van de Heyning, P., 2007. Validation of the Dutch and the French version of the Tinnitus Questionnaire. B-ENT 3 (Suppl. 7), 11–17.
Meeus, O., Heyndrickx, K., Lambrechts, P., De Ridder, D., Van de Heyning, P., 2010. Phase-shift treatment for tinnitus of cochlear origin. Eur. Arch. Otorhinolaryngol. 267 (6), 881–888.
Meeus, O., De Ridder, D., Van de Heyning, P., 2011. Administration of the combination Clonazepam-Deanxit as treatment for tinnitus. Otol. Neurotol. 32 (4), 701–709.
Mohan, A., Vanneste, S., 2017. Adaptive and maladaptive neural compensatory consequences of sensory deprivation—from a phantom percept perspective. Prog. Neurobiol. 153, 1–17.
Mohan, A., De Ridder, D., Vanneste, S., 2016a. Emerging hubs in phantom perception connectomics. NeuroImage Clin. 11, 181–194.
Mohan, A., De Ridder, D., Vanneste, S., 2016b. Graph theoretical analysis of brain connectivity in phantom sound perception. Sci. Rep. 6, 19683.
Moisset, X., Bouhassira, D., 2007. Brain imaging of neuropathic pain. NeuroImage 37, S80–S88.
Oken, B.S., Chamine, I., Wakeland, W., 2015. A systems approach to stress, stressors and resilience in humans. Behav. Brain Res. 282, 144–154.
Park, J.E., Jung, S.C., Ryu, K.H., Oh, J.Y., Kim, H.S., Choi, C.-G., Kim, S.J., Shim, W.H., 2017. Differences in dynamic and static functional connectivity between young and elderly healthy adults. Neuroradiology 59, 781–789.
Pascual-Marqui, R.D., 2002. Standardized low-resolution brain electromagnetic tomography (sLORETA): technical details. Methods Find. Exp. Clin. Pharmacol. 24 (Suppl D), 5–12.
Rubinov, M., Sporns, O., 2010. Complex network measures of brain connectivity: uses and interpretations. NeuroImage 52, 1059–1069.
Russo, S.J., Murrough, J.W., Han, M.-H., Charney, D.S., Nestler, E.J., 2012. Neurobiology of resilience. Nat. Neurosci. 15, 1475–1484.
Sanz-Arigita, E.J., Schoonheim, M.M., Damoiseaux, J.S., Rombouts, S.A., Maris, E., Barkhof, F., Scheltens, P., Stam, C.J., 2010. Loss of 'small-world' networks in Alzheimer's disease: graph analysis of FMRI resting-state functional connectivity. PLoS One 5, e13788.
Scheffer, M., Carpenter, S.R., Dakos, V., van Nes, E.H., 2015. Generic indicators of ecological resilience: inferring the chance of a critical transition. Annu. Rev. Ecol. Evol. Syst. 46, 145–167.
Selye, H., 1946. The general adaptation syndrome and the diseases of adaptation 1. J. Clin. Endocrinol. Metab. 6, 117–230.

Shanahan, M., 2010. Metastable chimera states in community-structured oscillator networks. Chaos 20, 013108.
Song, J.-J., De Ridder, D., Schlee, W., Van de Heyning, P., Vanneste, S., 2013. "Distressed aging": the differences in brain activity between early-and late-onset tinnitus. Neurobiol. Aging 34, 1853–1863.
Song, J.-J., Vanneste, S., Schlee, W., Van de Heyning, P., De Ridder, D., 2015. Onset-related differences in neural substrates of tinnitus-related distress: the anterior cingulate cortex in late-onset tinnitus, and the frontal cortex in early-onset tinnitus. Brain Struct. Funct. 220, 571–584.
Sporns, O., Zwi, J.D., 2004. The small world of the cerebral cortex. Neuroinformatics 2, 145–162.
Supekar, K., Uddin, Lucina Q., Khouzam, A., Phillips, J., Gaillard, William D., Kenworthy, Lauren E., Yerys, Benjamin E., Vaidya, Chandan J., Menon, V., 2013. Brain hyperconnectivity in children with autism and its links to social deficits. Cell Rep. 5, 738–747.
Tognoli, E., Kelso, J.A., 2014. The metastable brain. Neuron 81, 35–48.
Vanneste, S., Plazier, M., der Loo, E., de Heyning, P.V., Congedo, M., De Ridder, D., 2010a. The neural correlates of tinnitus-related distress. NeuroImage 52, 470–480.
Vanneste, S., Plazier, M., Van Der Loo, E., Van de Heyning, P., De Ridder, D., 2010b. The differences in brain activity between narrow band noise and pure tone tinnitus. PLoS One 5, e13618.
Vanneste, S., Van de Heyning, P., De Ridder, D., 2011. Contralateral parahippocampal gamma-band activity determines noise-like tinnitus laterality: a region of interest analysis. Neuroscience 199, 481–490.
Vanneste, S., Congedo, M., De Ridder, D., 2014. Pinpointing a highly specific pathological functional connection that turns phantom sound into distress. Cereb. Cortex 24, 2268–2282.
Váša, F., Shanahan, M., Hellyer, P.J., Scott, G., Cabral, J., Leech, R., 2015. Effects of lesions on synchrony and metastability in cortical networks. NeuroImage 118, 456–467.
Wager, T.D., Atlas, L.Y., Lindquist, M.A., Roy, M., Woo, C.-W., Kross, E., 2013. An fMRI-based neurologic signature of physical pain. N. Engl. J. Med. 368, 1388–1397.
Walker, B., Holling, C.S., Carpenter, S.R., Kinzig, A., 2004. Resilience, adaptability and transformability in social–ecological systems. Ecol. Soc. 9, 5.
Watts, D.J., Strogatz, S.H., 1998. Collective dynamics of 'small-world' networks. Nature 393, 440–442.
Weisz, N., Moratti, S., Meinzer, M., Dohrmann, K., Elbert, T., 2005. Tinnitus perception and distress is related to abnormal spontaneous brain activity as measured by magnetoencephalography. PLoS Med. 2, e153.
White, T.P., Joseph, V., Francis, S.T., Liddle, P.F., 2010. Aberrant salience network (bilateral insula and anterior cingulate cortex) connectivity during information processing in schizophrenia. Schizophr. Res. 123, 105–115.
Whitfield-Gabrieli, S., Thermenos, H.W., Milanovic, S., Tsuang, M.T., Faraone, S.V., McCarley, R.W., Shenton, M.E., Green, A.I., Nieto-Castanon, A., LaViolette, P., 2009. Hyperactivity and hyperconnectivity of the default network in schizophrenia and in first-degree relatives of persons with schizophrenia. Proc. Natl. Acad. Sci. 106, 1279–1284.